

Novel Thienopyrimidine-Based PET Tracers for P2Y₁₂ Receptor Imaging in the Brain

Berend van der Wildt,* Bienneke Janssen, Aleksandra Pekořak, E. Johanna L. Stéen, Robert C. Schuit, Esther J. M. Kooijman, Wissam Beaino, Danielle J. Vugts, and Albert D. Windhorst

Cite This: *ACS Chem. Neurosci.* 2021, 12, 4465–4474

Read Online

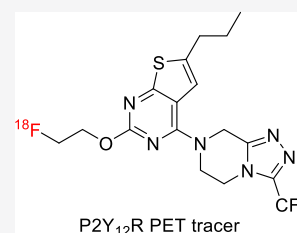
ACCESS |

Metrics & More

Article Recommendations

Supporting Information

ABSTRACT: The P2Y₁₂ receptor (P2Y₁₂R) is uniquely expressed on microglia in the brain, and its expression level directly depends on the microglial activation state. Therefore, P2Y₁₂R provides a promising imaging marker for distinguishing the pro- and anti-inflammatory microglial phenotypes, both of which play crucial roles in neuroinflammatory diseases. In this study, three P2Y₁₂R antagonists were selected from the literature, radiolabeled with carbon-11 or fluorine-18, and evaluated in healthy Wistar rats. Brain imaging was performed with and without blocking of efflux transporters *P*-glycoprotein and breast cancer resistance protein using tariquidar. Low brain uptake in healthy rats was observed for all tracers at baseline conditions, whereas blocking of efflux transporters resulted in a strong (6–7 fold) increase in brain uptake for both of them. Binding of the most promising tracer, [¹⁸F]3, was further evaluated by in vitro autoradiography on rat brain sections, ex vivo metabolite studies, and in vivo P2Y₁₂R blocking studies. In vitro binding of [¹⁸F]3 on rat brain sections indicated high P2Y₁₂R targeting with approximately 70% selective and specific binding. At 60 min post-injection, over 95% of radioactivity in the brain accounted for an intact tracer. In blood plasma, still 40% intact tracer was found, and formed metabolites did not enter the brain. A moderate P2Y₁₂R blocking effect was observed in vivo by positron emission tomography (PET) imaging with [¹⁸F]3 (*p* = 0.04). To conclude, three potential P2Y₁₂R PET tracers were obtained and analyzed for P2Y₁₂R targeting in the brain. Unfortunately, the brain uptake appeared low. Future work will focus on the design of P2Y₁₂R inhibitors with improved physicochemical characteristics to reduce efflux transport and increase brain penetration.



KEYWORDS: P2Y₁₂ receptor (P2Y₁₂R), PET imaging, neuroinflammation, microglia, anti-inflammatory phenotype

INTRODUCTION

Microglia are the resident immune cells of the central nervous system (CNS), and in the adult brain, they carry out surveillance functions to maintain homeostasis.^{1–3} Microglia are the first line of defense in the brain, and upon tissue injury and infiltration of disease pathogens, microglia undergo cellular activation. This activation is characterized by morphological and functional changes including alteration in cell surface receptors and cytokine and chemokine secretion.³ The activation process is marked by the secretion of pro-inflammatory cytokines and chemokines such as IL1 β , IL-6, and TNF α , together with nitric oxide reactive oxygen species. In an acute event, the mounted neuroinflammation tends to resolve when the damage is repaired, resulting in shifting of microglia to an anti-inflammatory and reparative phenotype. However, in neurodegenerative diseases such as Alzheimer's disease, Parkinson's disease, Huntington's disease, and multiple sclerosis, but also after trauma, neuroinflammation tends to become a chronic process that leads to a variety of microglia phenotypes that contribute to excessive neuronal damage and become a major driver of the disease.^{4–6} Since anti-inflammatory microglia promote regeneration and repair mechanism, numerous novel experimental therapies are focusing on modulating microglia activation from a pro-

inflammatory phenotype to a resting or even anti-inflammatory phenotype in order to harness their regenerative potential.^{7,8}

Positron emission tomography (PET) is already used clinically for imaging of neuroinflammation by targeting the 18 kDa translocator protein (TSPO), and development of improved TSPO PET tracers is continuously ongoing.⁹ Although TSPO imaging has proven to image inflammation, it has several limitations. TSPO is not specifically expressed on microglia but also expressed on other cells in the brain such as astrocytes and endothelial cells.¹⁰ Furthermore, TSPO over-expression does not discriminate between pro- and anti-inflammatory phenotypes. Finally, genetic polymorphisms and the presence of low and high binders complicate PET data interpretation. Therefore, PET tracers for more specific biomarkers are essential.^{10,11} The next-generation PET tracers for specifically imaging activated microglia in the pro-inflammatory state bind to the P2X₇ receptor. These tracers

Received: September 29, 2021

Accepted: November 1, 2021

Published: November 10, 2021



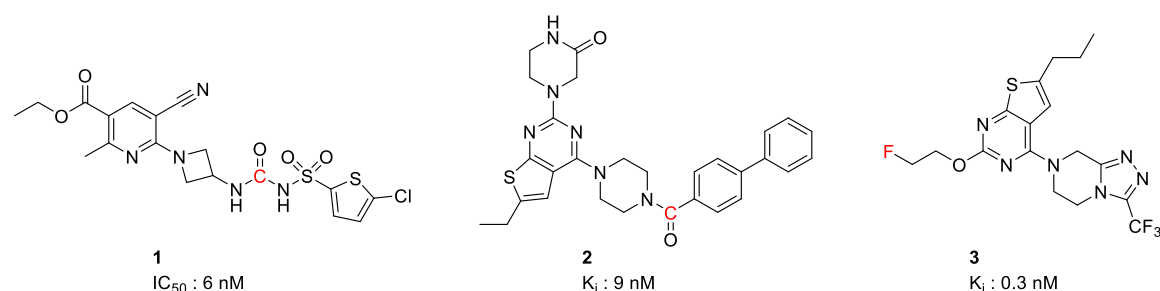
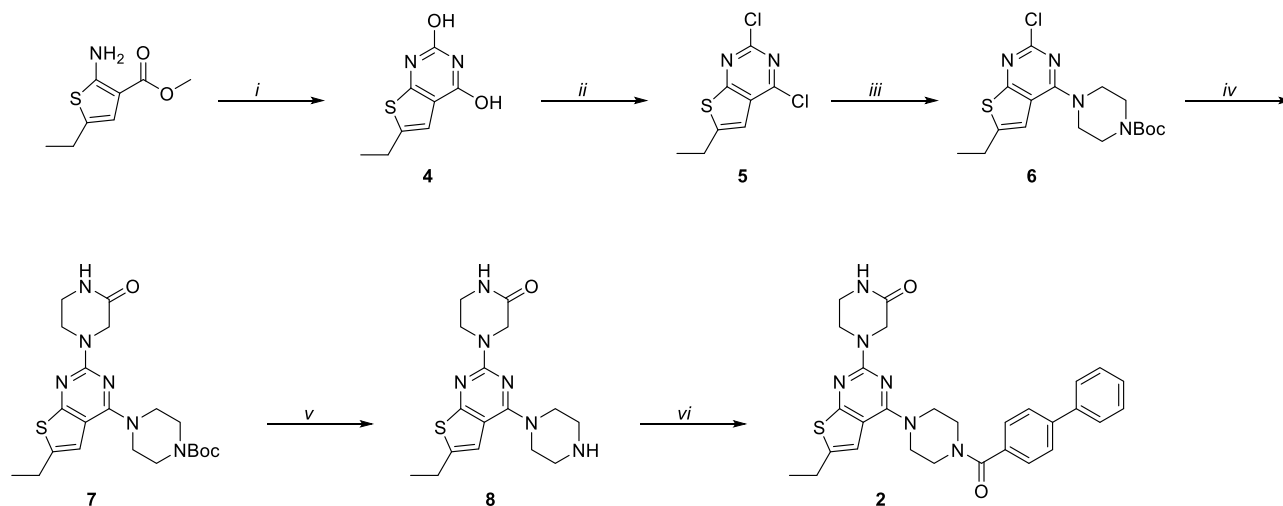


Figure 1. P2Y₁₂R antagonists studied in this work.^{20,25,26} The positions of the PET radiolabels carbon-11 and fluorine-18 are indicated in red.

Scheme 1. Synthesis of the P2Y₁₂R Antagonist 2 and the Labeling Precursor Molecule 8^a



^aReagents and conditions: (i) Potassium cyanate, acetic acid, rt, 16 h, then KOH, water, reflux, 2.5 h, and 59%; (ii) phenylphosphonic dichloride (neat), 150 °C, 2.5 h, and 30%; (iii) Boc-piperazine, DIPEA, dichloromethane/tetrahydrofuran (DCM/THF), rt, 5 h, and 81%; (iv) piperazin-2-one, DIPEA, NMP, 105 °C, 16 h, and 61%; (v) HCl (4 M in dioxane, rt, 1 h; 88%; and (vi) 4-phenylbenzoyl chloride, DIPEA, DMF, rt, 4 h, and 66%.

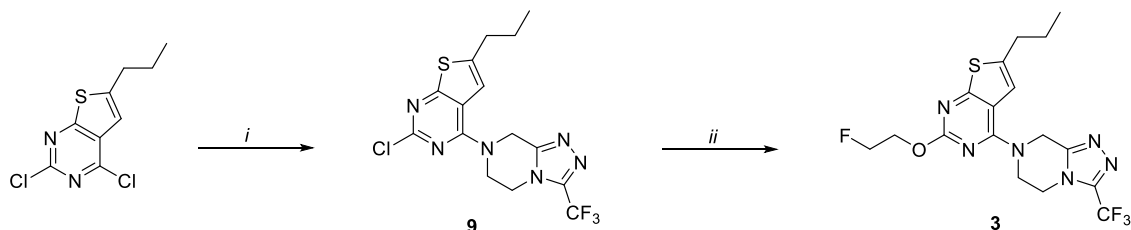
have recently been used for the imaging of activated microglia in vivo in animal models and human multiple sclerosis patients.^{12–19} Another purinergic receptor, P2Y₁₂R, was recently identified as a specific marker for the anti-inflammatory phenotype.²⁰ P2Y₁₂R is a G-protein coupled receptor that is uniquely expressed on microglia in the brain.²¹ P2Y₁₂R has an ADP binding site at the extracellular domain, a binding site to which many P2Y₁₂R antagonists bind as well.^{22,23} The selective downregulation of P2Y₁₂R expression on pro-inflammatory microglia and its upregulation on anti-inflammatory microglia position P2Y₁₂R as an attractive target for PET tracer development.²⁴ In fact, the first P2Y₁₂R PET tracer (Figure 1, compound 1) was already reported and validated in vitro on both rat and human brain sections.²⁰ However, the compound failed to enter the brain, thereby limiting its use for in vivo brain imaging. The focus of the current work is to develop brain penetrating P2Y₁₂R PET tracers. This effort would lead to having access to PET tracers for imaging both the pro- and anti-inflammatory activation states, which will contribute in better understanding of the role of activated microglia during disease progression and in the development of novel treatment strategies aiming at modulating the immune response in the brain.^{10,11} We selected two leads from the patent literature, compounds 2 and 3, both of which are high-affinity thienopyrimidine-based P2Y₁₂R inhibitors, that allow for radiolabeling with either carbon-11 or fluorine-18 (Figure 1).^{25,26} Compounds 2 and 3 have a

reported K_i value of 9 and 0.3 nM, respectively, as determined in a competitive binding assay employing human P2Y₁₂R-transfected HEK cells and labeled 2-methylthio-adenosine-5'-diphosphate as a substrate. The proposed labeling positions for compounds 2 and 3 are depicted in red.

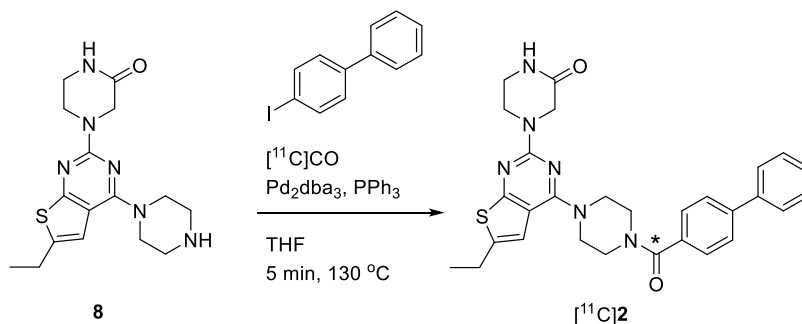
RESULTS AND DISCUSSION

Motivation of the Work. Currently, no validated PET tracer for imaging of P2Y₁₂R exists. The first and only attempt published so far concerns a PET tracer that, based on the ex vivo biodistribution results, appears to not enter the brain in healthy rats.²⁰ In the current study, this finding is re-evaluated by means of dynamic PET scanning with this tracer. Additionally, two other potent P2Y₁₂R antagonists are radiolabeled and evaluated for brain uptake and P2Y₁₂R binding in rats. Lack of brain uptake is further studied by blocking efflux transporters at the blood–brain barrier (BBB). Together, this study should contribute to an increased understanding of the behavior of P2Y₁₂R PET tracers toward the development a clinical candidate for future studies.

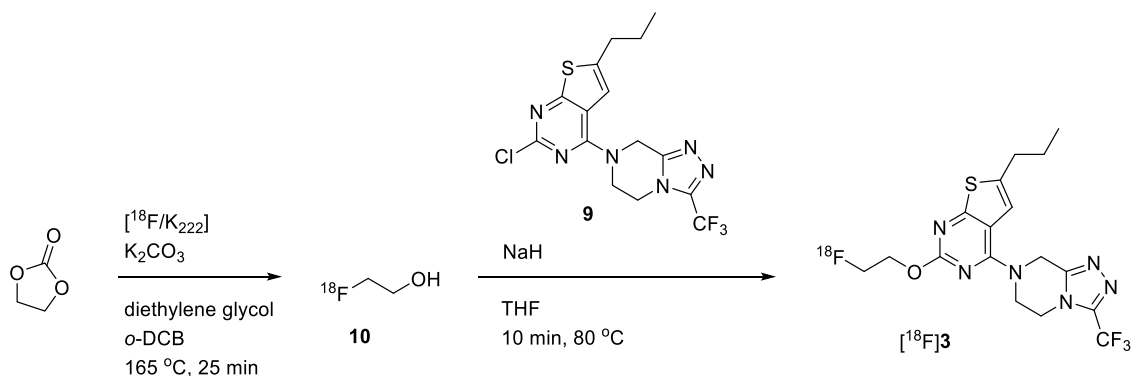
Synthesis of Reference Compounds and Labeling Precursor Molecules. The synthesis of the P2Y₁₂R antagonist 2 and the corresponding labeling precursor molecule 8 was performed according to a previously described method (Scheme 1).²⁵ Aminothiophene carboxylate was reacted with potassium cyanate to obtain 2,4-diol pyrimidyl heterocycle 4. The alcohol groups were converted to chlorides

Scheme 2. Synthesis of the P2Y₁₂R Antagonist 3 and the Labeling Precursor Molecule 9^a

^aReagents and conditions: (i) 3-(trifluoromethyl)-5,6,7,8-tetrahydro-[1,2,4]triazolo[4,3-a]pyrazine·HCl, DIPEA, DMF, 100 °C, 16 h, and 82% and (ii) 2-fluoroethanol, Pd(OAc)₂, BINAP, Cs₂CO₃, toluene, reflux, 4 h, and 17%

Scheme 3. One-Step Radiosynthesis of [¹¹C]2^a

^aReagents and conditions: [¹¹C]CO, biphenyl iodide, Pd₂dba₃, PPh₃, THF, 5 min, 130 °C, and 10 ± 3% (d.c.). The position of the carbon-11 label is depicted with *.

Scheme 4. Two-step Radiosynthesis of [¹⁸F]3^a

^aReagents and conditions: (i) ¹⁸F⁻, K₂₂₂, K₂CO₃, diethylene glycol/1,2-dichlorobenzene (1:4), 25 min, 165 °C, and 89 ± 2% and (ii) precursor 9, NaH, THF, 20 min, 60 °C, and 35 ± 8%.

by reacting with phenylphosphonic dichloride to obtain chloropyrimidine 5. Amination using Boc-piperazine afforded 6, and a subsequent amination under harsher conditions resulted in pyrimidine 7. Acid-mediated Boc-deprotection followed by an alkaline workup resulted in the piperazine derivative 8, which was used as the precursor for radiolabeling. Coupling of 8 with 4-phenylbenzoyl chloride afforded the reference compound 2 in an overall yield of 6.5% over six reaction steps.

The P2Y₁₂R antagonist 3 was obtained by amination of the dichloropyrimidine with pyrazolotriazine to obtain compound 9, which was used as a precursor for fluorine-18 labeling. The reference compound 3 was subsequently obtained by palladium-catalyzed C–O bond formation with 2-fluoroethanol (Scheme 2).

Radiosynthesis of [¹¹C]1, [¹¹C]2, and [¹⁸F]3. The PET tracer [¹¹C]1 was synthesized as described previously²⁰ and was obtained in a radiochemical yield of 17 ± 4% (based on [¹¹C]CO₂, decay-corrected to start the synthesis, 966 ± 208 MBq) in a total synthesis time of 45 min. The radiochemical purity was >99%, and the molar activity was 82 ± 28 GBq/μmol (*n* = 3). The PET tracer [¹¹C]2 was obtained by a Pd-mediated aminocarbonylation with [¹¹C]CO as the synthon (Scheme 3). The THF-soluble carrier gas xenon was used for quantitative transfer of [¹¹C]CO into the sealed reaction vial with minimal pressure build-up.²⁷ Using a Pd₂dba₃ and PPh₃ ligand system in THF and a reaction time of 5 min at 130 °C resulted in the formation of [¹¹C]2. Starting the procedure with approximately 25 GBq of [¹¹C]CO₂, compound [¹¹C]2 could be obtained in a radiochemical yield of 10 ± 3% (based on [¹¹C]CO₂, decay-corrected to start the synthesis) in a total

synthesis time of 40 min. After formulation, 578 ± 93 MBq of product was obtained with a radiochemical purity of >99% and a molar activity of 93 ± 49 GBq/ μmol ($n = 3$).

Efforts to obtain the PET tracer [^{18}F]3 in a one-step procedure by nucleophilic substitution with fluorine-18 were unsuccessful due to precursor instability. Therefore, a two-step approach using 2-[^{18}F]fluoroethanol was selected.²⁸ As such, [^{18}F]3 was synthesized in a two-step, two-pot building block strategy as depicted in Scheme 4. First, 2-[^{18}F]fluoroethanol was synthesized from ethylenecarbonate following a previously reported procedure with small adaptation.²⁸ 2-[^{18}F]fluoroethanol, which was obtained in an $89 \pm 2\%$ yield, was distilled at 165°C under a gentle helium flow (10 mL/min) to a second reaction vial. Palladium-mediated C–O bond formation in this second reaction vial using conditions similar to unlabeled 3 (Scheme 2) resulted in [^{18}F]3 in low and poorly reproducible conversions of $4 \pm 4\%$ [$n = 3$, conversion based on analytical high-performance liquid chromatography (HPLC)]. Williamson ether synthesis using NaH in THF toward [^{18}F]3 resulted in improved radiochemical yields up to 10%, while precursor 9 was cleanly converted to a more polar non-radioactive compound based on analytical HPLC. It was suspected that despite its high boiling point of 244°C , small amounts of diethyleneglycol were distilled together with 2-[^{18}F]fluoroethanol to the second etherification vial. Diethylene glycol then competes with 2-[^{18}F]fluoroethanol in the subsequent nucleophilic aromatic substitution reaction, thereby consuming precursor 9 and causing poor radiochemical yields. Indeed, changing solvent to a mixture of 1,2-dichlorobenzene and diethyleneglycol (4:1, v/v) in the 2-[^{18}F]fluoroethanol generation step resulted in conversions to [^{18}F]3 of up to 50% without compromising the 2-[^{18}F]fluoroethanol yield (Supporting Information Figure S1). Starting with approximately 20 GBq of fluorine-18, [^{18}F]3 was obtained in a $9 \pm 2\%$ radiochemical yield (decay-corrected to start the synthesis) in a total synthesis time of 90 min. The isolated radioactivity amount was 958 ± 44 MBq, and the molar activity was 70 ± 14 GBq/ μmol at the end of the synthesis. The radiochemical purity was >99%, and no chemical contaminants were observed ($n = 3$) (Supporting Information Figure S2).

Lipophilicity. The distribution coefficients of [^{11}C]2 and [^{18}F]3 at physiological pH ($\log D_{7.4}$) were determined by the shake flask method as 2.66 ± 0.10 and 2.06 ± 0.01 , respectively ($n = 3$). The $\log D_{7.4}$ of [^{11}C]1 was previously determined as 1.93 ± 0.02 using the same method. All values are well within the preferred range for BBB penetration.

In Vivo Evaluation of PET Tracers. The brain uptake of all the three P2Y₁₂R PET tracers was evaluated in vivo in wild-type Wistar rats using PET imaging. In addition, the dominant efflux transporters P-glycoprotein and breast cancer resistance protein were blocked with tariquidar to determine the efflux substrate behavior.^{29,30} In an earlier study, the first reported P2Y₁₂R PET tracer ([^{11}C]1 in Figure 1) demonstrated good binding properties on brain sections in vitro, but in an ex vivo biodistribution experiment, the tracer failed to enter the rat brain after intravenous (iv) administration.²⁰ However, this apparent lack of brain uptake was determined statically at 5 and 15 min post-injection. By performing dynamic PET scanning instead of ex vivo biodistribution, time–activity curves with higher temporal resolution could be generated. Indeed, low brain uptake for [^{11}C]1 was observed at each time point [Figure 2, SUV_{max} 0.1 (after the initial perfusion peak), n

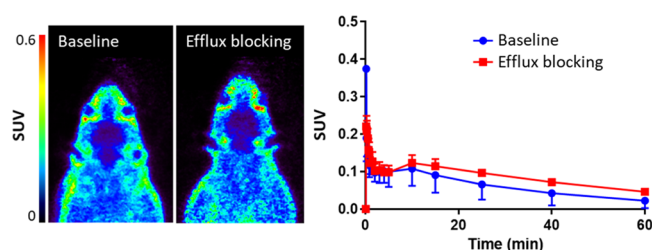


Figure 2. PET imaging results of [^{11}C]1 in healthy Wistar rats at baseline and efflux transporter blocking conditions. Left: representative PET images (cross sections summed over 60 min). Right: time–activity curves following the administration of [^{11}C]1 to healthy Wistar rats at baseline or efflux transporter blocking conditions. Error bars represent the standard deviation ($n = 2$ per group).

$= 2$], corresponding with the previously reported biodistribution data (%ID/g in rat brain <0.1).²⁰ Blocking of efflux transporters did not dramatically increase the brain uptake [SUV_{max} 1.2 (after the initial perfusion peak), $n = 2$, the area under the curves are 3.8 ± 0.7 and 5.2 ± 0.2 for baseline and efflux transporter blocking conditions, respectively]. Therefore, it was concluded that [^{11}C]1 does not pass the BBB due to its unfavorable physicochemical properties. Specifically, the sulfonylurea presents a functional group with a large polar surface area. Due to the structural overlap with other P2Y₁₂R antagonists from the same compound class,^{31,32} translating any of these analogue structures into PET tracers for imaging of P2Y₁₂R expression in the brain is discouraged.

Similar to [^{11}C]1, the tracer [^{11}C]2 also did not pass the BBB under baseline conditions [Figure 3, SUV_{max} 0.04 (after the initial perfusion peak); area under the curve 2.4 ± 0.1]. Upon pretreatment of rats with tariquidar, a strong increase in brain uptake was observed (SUV_{max} 0.25; area under the curve 14.2 ± 1.2). However, this increase was accompanied by a general 2–3-fold increase in radioactivity concentrations throughout the rat (Figure 3). This indicates a delayed washout in addition to an increase in brain uptake, hinting at a tariquidar-mediated increased availability of [^{11}C]2 or a reduction of [^{11}C]2 washout from the blood. Moreover, no washout from the brain was observed. Because of these generally non-favorable kinetics of [^{11}C]2, no further experiments were conducted with this compound.

Compound [^{18}F]3 also did not show brain uptake at baseline conditions (Figure 4, SUV_{max} : 0.2; area under the curve 4.4 ± 0.1). However, in contrast to [^{11}C]1 and 2, a strong increase in brain uptake was observed upon blocking of efflux transporters, followed by clearance from the brain (SUV_{max} : 1.0; area under the curve 27.6 ± 1.1). Unlike [^{11}C]2, no general increase of radioactivity concentrations in other organs was observed (Figure 4, left image).

The observed brain uptake of each tested PET tracer corresponds well with the calculated CNS-MPO scores (a qualitative measure for the prediction of brain uptake) for each of the compounds, with compound 3 being the only compound scoring above 4³³ [Supporting Information Figures S4–S6: scoring of 3.5 for compound 1; 2.6 for compound 2; and 4.5 for compound 3 (the maximum score is 6, and the threshold is commonly defined as ≥ 4)]. Using CNS-PET-MPO scoring, each of the compounds scored poorly [Supporting Information Figure S4–S6: scoring of 2.6 for compound 1; 2.0 for compound 2; and 2.5 for compound 3 (the maximum score is 6, and the threshold is commonly

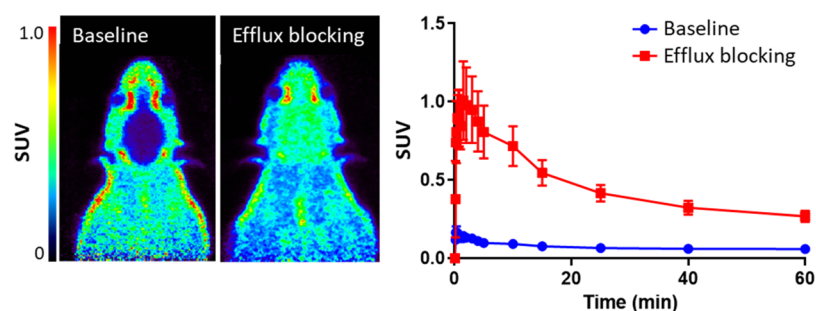


Figure 3. PET imaging results of $[^{11}\text{C}]2$ in healthy Wistar rats at baseline and efflux transporter blocking conditions. Left: representative PET images (cross sections summed over 60 min). Right: time–activity curves following the administration of $[^{11}\text{C}]2$ to healthy Wistar rats at baseline or efflux transporter blocking conditions. Error bars represent the standard deviation ($n = 2$ per group).

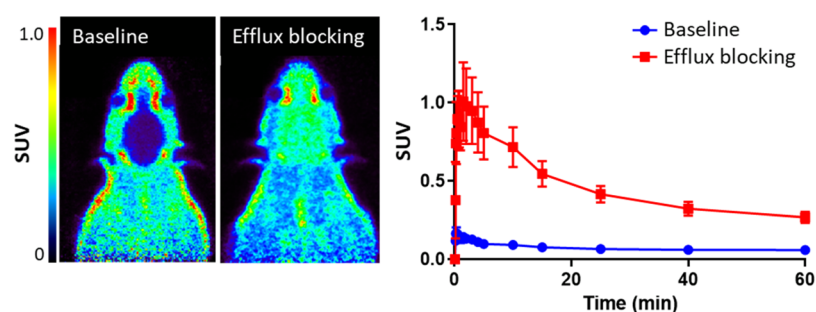


Figure 4. PET imaging results of $[^{18}\text{F}]3$ in healthy Wistar rats at baseline and efflux transporter blocking conditions. Left: representative PET images (cross sections summed over 60 min). Right: time–activity curves following the administration of $[^{18}\text{F}]3$ to healthy Wistar rats at baseline or efflux transporter blocking conditions. Error bars represent the standard deviation ($n = 2$ per group).

defined as ≥ 3).³⁴ Unfortunately, compound 3 appeared to be a strong substrate for efflux transporters. *In silico* predictions on whether small molecules are efflux transporter substrates suffer from inaccuracy, largely because of the various efflux transporters expressed in the brain capillary endothelial cells in combination with many pharmacokinetic parameters that should be considered. In practice, minor modifications to a molecule can have drastic effects on the efflux rate of a compound. Moreover, efflux transporters are commonly less active in higher species.³⁵ As a result, PET tracers that suffer from efflux transport in rodents might eventually provide adequate brain uptake in humans. To avoid premature discarding of PET tracers for human application as a result of efflux transport in rodents, design of imaging experiments with blocking of efflux transporters is strongly encouraged.³⁶ Therefore, despite being an efflux transporter substrate, additional studies with $[^{18}\text{F}]3$ were performed to further understand the behavior of the compound *in vitro* and *in vivo*. Due to the undesired *in vivo* behavior of compound $[^{11}\text{C}]2$, no further experiments were performed with this PET tracer.

In Vitro Autoradiography, Metabolite Analysis, and In Vivo PET Imaging with $[^{18}\text{F}]3$ in Combination with Efflux Transporter Blocking and P2Y₁₂R Blocking. *In vitro* autoradiography on rat brain sections was performed to validate the binding specificity of $[^{18}\text{F}]3$ to brain tissue (Figure 5). Highly specific and selective binding was found, with blocking efficiencies of about 70% when co-incubating with an excess of unlabeled 3 or with the structurally non-related P2Y₁₂R antagonist 1 (both inhibitors used at 1 μM). Blocking with antagonist 1 demonstrated very little non-selective binding (<10%). Binding was homogeneous throughout the brain, as expected based on the widespread distribution of resting state microglia in healthy rats.

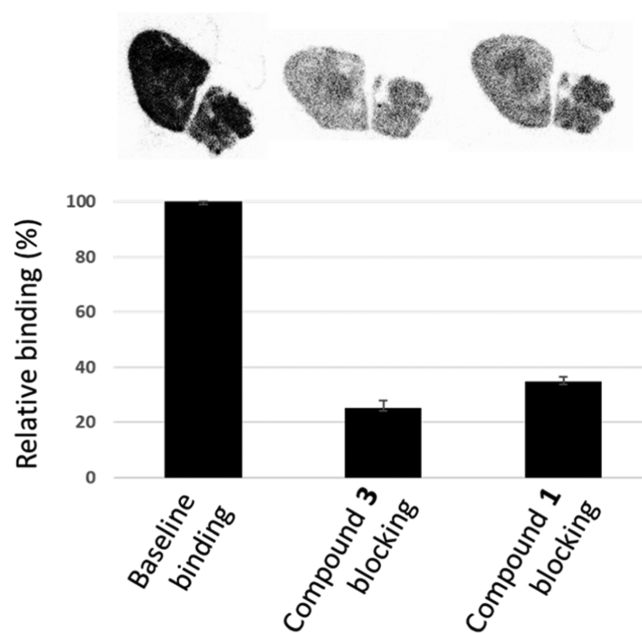


Figure 5. *In vitro* autoradiography on rat brain sections using $[^{18}\text{F}]3$. Top: representative autoradiography images at baseline and blocking conditions (self-blocking and blocking using compound 1). Inhibitors were co-incubated at 1 μM concentration. Bottom: quantification of $[^{18}\text{F}]3$ binding. The results are expressed as average \pm standard deviation ($n = 3$).

To determine specific binding to P2Y₁₂R in the rat brain *in vivo*, another PET imaging experiment was performed. In this case, the first group of rats ($n = 4$) received tariquidar for blocking of efflux transporters, followed by administration of $[^{18}\text{F}]3$. The second group received both tariquidar and

unlabeled compound **3** for blocking of P2Y₁₂R prior to scanning with [¹⁸F]**3** (Figure 6). Obviously, selective and non-

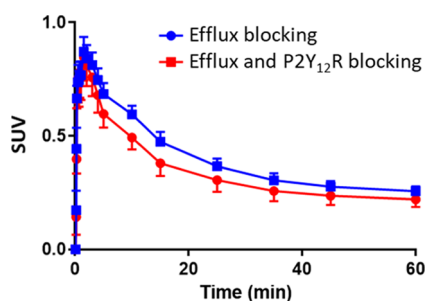


Figure 6. Whole brain time–activity curves following the administration of [¹⁸F]**3**. Rats received either tariquidar + tracer (blue line) or tariquidar + unlabeled **3** and tracer (red line). Error bars indicate the standard deviation ($n = 4$ per group).

specific binding cannot be tested by self-blocking, as that would require the use of a structurally different P2Y₁₂R antagonist. However, no such P2Y₁₂R antagonist that enters the brain is currently available as commonly these compounds have been developed as antithrombotic drugs working outside of the CNS.³⁷ Blocking of P2Y₁₂R with unlabeled **3** resulted in a significant decrease in brain SUVs throughout the entire scan time (area under the curve 24.1 ± 0.5 and 20.6 ± 0.7 for baseline and blocking, respectively, $p = 0.04$). The blocking effect in brain uptake was confirmed by the post-scanning *ex vivo* biodistribution (Supporting Information Figure S7). It should be taken into account that P2Y₁₂R is only expressed in baseline amounts in the healthy brain, and as such, it is conceivable that in animal models of P2Y₁₂R overexpression, the specific binding and blocking effect in brain would be significantly higher.³⁸ Determination of the metabolites in the brain after the PET scan demonstrated that >90% of the tracer was still intact, indicating that hardly any radioactive metabolites are present in the brain, which is beneficial for future applications. Blood radiometabolite analyses revealed the presence of two major radiometabolites in blood at 60 min post-injection, accounting for approximately 60% of total activity, as well as approximately 40% of intact tracer. Formation of radiometabolites from [¹⁸F]**3** was not affected by the co-administration of unlabeled **3** (Supporting Information Figure S3).

CONCLUSIONS

Two novel potential P2Y₁₂R PET tracers were obtained and evaluated *in vivo* in healthy rats. Compound [¹⁸F]**3** showed highly selective and specific binding on rat brain sections. Due to efflux transport, the brain uptake of each of the tracers in rats was low at baseline conditions, which limits their use in P2Y₁₂R imaging studies in rodents. However, further studies in higher species with lower efflux transporter activity are warranted. Additionally, future work will focus on the design of P2Y₁₂R antagonists with improved physicochemical properties to reduce efflux transport and increase brain penetration.

MATERIALS AND METHODS

General Procedure. All chemicals and reagents were obtained from Sigma-Aldrich (St. Louis, USA) with the exception of 2,4-dichloro-6-propylthieno[2,3-*d*]pyrimidine (Oxchem, Wood Dale IL, USA). Solvents were obtained from Biosolve (Valkenswaard, the Netherlands) and used as received unless stated otherwise. Reaction

monitoring by thin-layer chromatography (TLC) was performed on pre-coated silica 60 F254 aluminum plates (Merck, Darmstadt, Germany). Spots were visualized by UV light, KMnO₄, or ninhydrin staining. Evaporation of solvents was performed under reduced pressure at 40 °C using a rotary evaporator (Buchi, Flawil, Switzerland). Flash column chromatography was performed manually using Silica gel 60 Å (Merck, Darmstadt, Germany). Nuclear magnetic resonance (NMR) spectroscopy was performed using a Bruker (Billerica, MA, USA) AVANCE 500 (500.27 MHz for ¹H and 125.81 MHz for ¹³C) with chemical shifts (δ) reported in parts per million (ppm) relative to the solvent (chloroform (CDCl₃), ¹H 7.26 ppm, ¹³C 77.16 ppm, and DMSO-*d*₆, ¹H 2.50 ppm, ¹³C 39.52 ppm). Electrospray ionization high-resolution mass spectrometry (ESI-HRMS) was carried out using a Bruker microTOF-Q in the positive ion mode (capillary potential of 4500 V). For radio-TLC and autoradiography experiments, the TLC plates or brain sections were exposed to a phosphor imaging screen (GE Healthcare, Buckinghamshire, UK) and developed on a Typhoon FLA 7000 phosphor imager (GE Healthcare). Visualization of binding was performed using ImageQuantTL v8.1.0.0 (GE Healthcare). The radiochemistry nomenclature guidelines were followed.³⁹

6-Ethylthieno[2,3-*d*]pyrimidine-2,4-diol (4). A solution of potassium cyanate (3.76 g, 46.3 mmol) in water (20 mL) was added dropwise to a stirred solution of methyl 2-amino-5-ethylthiophene-3-carboxylate (3.08 g, 16.7 mmol) in acetic acid (54 mL), and the reaction was left to stir at rt for 16 h. The reaction mixture was poured in ice water (100 mL), and the resulting brown precipitate was collected by filtration, washed with ice water (40 mL), and subsequently heated to reflux (100 °C) in aqueous NaOH (0.67 g, 17 mmol in 50 mL water) for 2.5 h. After cooling to rt, the reaction mixture was cooled on ice, and the pH was adjusted to 6 using concentrated HCl. The precipitate was collected by filtration, washed with ice water (2 × 25 mL), and subsequently dried for 16 h *in vacuo* to yield compound **4** as a white solid (1.92 g, 9.78 mmol, 59%). ¹H NMR (500.27 MHz, DMSO-*d*₆): δ 10.85 (bs, 1H), 8.34 (s, 1H), 6.80 (s, 1H), 2.70 (q, 2H, $J = 7.5$ Hz), 1.20 (t, 3H, $J = 7.5$ Hz); ¹³C NMR (125.81 MHz, DMSO-*d*₆): δ 159.46, 153.54, 151.71, 136.41, 117.18, 114.11, 22.59, 15.37; ESI-HRMS: calcd for C₈H₉N₂O₂S [M + H]⁺, 197.0379; found, 197.0346.

2,4-Dichloro-6-ethylthieno[2,3-*d*]pyrimidine (5). A mixture of compound **4** (1.92 g, 9.78 mmol) and phenylphosphonic dichloride (19.0 mL, 135 mmol) was heated at 150 °C for 2.5 h. The mixture was cooled on ice, and sat. NaHCO₃ (800 mL) was added in portions. After neutralization, the aqueous layer was extracted with DCM (3 × 100 mL). The combined organic fractions were dried over Na₂SO₄ and concentrated *in vacuo*. Flash column chromatography (Hex/EtOAc 7:3) yielded compound **5** as a white solid (0.68 g, 2.9 mmol, 30%). ¹H NMR (500.27 MHz, CDCl₃): δ 7.11 (s, 1H), 3.03 (q, 2H, $J = 7.5$ Hz), 1.44 (t, 3H, $J = 7.5$ Hz); ¹³C NMR (125.81 MHz, CDCl₃): δ 154.01, 153.43, 151.51, 129.23, 115.03, 24.75, 14.98; ESI-HRMS: calcd for C₈H₇Cl₂N₂S [M + H]⁺, 232.9702; found, 232.9694 [M + H]⁺.

tert-Butyl 4-(2-chloro-6-ethylthieno[2,3-*d*]pyrimidin-4-yl)piperazine-1-carboxylate (6). A solution of compound **5** (0.65 g, 2.8 mmol), Boc-piperazine (0.53 g, 2.8 mmol), and DIPEA (1.0 mL, 5.7 mmol) in THF (10 mL) and DCM (5 mL) was stirred at rt for 5 h. The mixture was concentrated *in vacuo*, and the residue was partitioned between DCM (25 mL) and brine (25 mL). The organic layer was dried over Na₂SO₄ and concentrated *in vacuo*. Flash column chromatography (Hex/EtOAc 8:2) was performed to yield compound **6** as a yellow solid (0.86 g, 2.3 mmol, 81%). ¹H NMR (500.27 MHz, CDCl₃): δ 6.97 (s, 1H), 3.93 (m, 4H), 3.63 (m, 4H), 2.94 (q, 2H, $J = 7.5$ Hz), 1.52 (s, 9H), 1.38 (t, 3H, $J = 7.5$ Hz); ¹³C NMR (125.81 MHz, CDCl₃): δ 169.96, 158.39, 154.78, 154.30, 144.41, 115.61, 115.47, 80.53, 28.54, 24.51, 15.54; ESI-HRMS: calcd for C₁₇H₂₄ClN₄O₂S [M + H]⁺, 383.1303; found, 383.1309.

tert-Butyl 4-(6-ethyl-2-(3-oxopiperazin-1-yl)thieno[2,3-*d*]pyrimidin-4-yl)piperazine-1-carboxylate (7). A solution of compound **6** (0.84 g, 2.2 mmol), piperazin-2-one (0.37 g, 3.7 mmol), and DIPEA (0.9 mL, 5.2 mmol) in NMP (10 mL) was heated

at 105 °C for 16 h. After cooling and diluting the mixture with EtOAc (100 mL), the organic fraction was washed with brine (100 mL). The organic layer was dried over Na₂SO₄ and concentrated in vacuo. Flash column chromatography (EtOAc) afforded the product **7** as a yellow solid (0.59 g, 1.3 mmol, 61%). ¹H NMR (500.27 MHz, CDCl₃): δ 6.79 (s, 1H), 6.60 (s, 1H), 4.42 (s, 2H), 4.06 (m, 2H), 3.80 (m, 4H), 3.58 (m, 4H), 3.48 (m, 2H), 2.83 (q, 2H, *J* = 7.5 Hz), 1.49 (s, 9H), 1.32 (t, 3H, *J* = 7.5 Hz); ¹³C NMR (125.81 MHz): δ 169.37, 158.50, 154.90, 115.57, 110.37, 80.35, 49.57, 48.69, 41.38, 30.81, 28.54, 24.34, 15.59; ESI-HRMS: calcd for C₂₁H₃₁N₆O₃S [M + H]⁺, 447.2173; found, 447.2155.

4-(6-Ethyl-4-(piperazin-1-yl)thieno[2,3-*d*]pyrimidin-2-yl)piperazin-2-one (8). A solution of compound **7** (0.52 g, 1.2 mmol) in DCM (8 mL) and 4 M HCl in 1,4 dioxane (4.0 mL, 16 mmol) was stirred at rt for 1 h. Hereafter, the mixture was concentrated in vacuo, followed by dilution with DCM (50 mL) and sat. NaHCO₃ (50 mL). The organic fraction was collected and dried over Na₂SO₄. After concentration in vacuo, compound **8** was obtained as a white solid (0.37 g, 1.1 mmol, 88%). ¹H NMR (500.27 MHz, CDCl₃): δ 6.80 (s, 1H), 6.18 (s, 1H), 4.45 (s, 2H), 4.04 (t, 2H, *J* = 5.5 Hz), 3.78 (t, 4H, *J* = 5.2 Hz), 3.48 (m, 2H), 3.00 (t, 4H, *J* = 4.9 Hz), 2.83 (q, 2H, *J* = 7.6 Hz), 1.32 (t, 3H, *J* = 7.5 Hz); ¹³C NMR (125.81 MHz, CDCl₃): δ 171.39, 169.36, 158.53, 157.11, 138.27, 115.51, 110.20, 49.45, 48.60, 47.39, 45.42, 41.33, 40.49, 30.70, 24.27, 15.48; ESI-HRMS: calcd for C₁₆H₂₂N₆O₃ [M + H]⁺, 347.1649; found, 347.1663.

4-(4-(4-([1,1'-Biphenyl]-4-carbonyl)piperazin-1-yl)-6-ethylthieno[2,3-*d*]pyrimidin-2-yl)piperazin-2-one (2). A solution of **8** (50 mg, 0.14 mmol), phenylbenzoyl chloride (37 mg, 0.17 mmol), and DIPEA (54 mg, 0.42 mmol) in DMF (2 mL) was stirred at rt for 4 h. After concentration in vacuo, the residue was purified by flash column chromatography (2% MeOH in DCM) to afford compound **2** as a yellow solid (50 mg, 66%). ¹H NMR (500.27 MHz, CDCl₃): δ 7.68 (d, 2H, *J* = 8.5 Hz), 7.62 (d, 2H, *J* = 7.61 Hz), 7.55 (d, 2H, *J* = 8.2 Hz), 7.48 (t, 2H, *J* = 7.48 Hz), 7.40 (7, 1H, *J* = 7.40 Hz), 6.79 (s, 1H), 6.40 (s, 1H), 4.42 (s, 2H), 4.05 (t, 2H, *J* = 5.2 Hz), 3.98–3.65 (m, 8H), 3.48 (m, 2H), 2.82 (q, 2H, *J* = 7.6 Hz), 1.33 (t, 3H, *J* = 7.7 Hz); ¹³C NMR (125.81 MHz, CDCl₃): δ 170.68, 169.33, 158.56, 143.15, 140.29, 134.14, 129.07, 129.04, 128.00, 127.93, 127.87, 127.46, 127.30, 115.32, 110.48, 48.67, 47.19, 41.36, 40.72, 24.36, 15.57; ESI-HRMS: calcd for C₂₉H₃₁N₆O₂S [M + H]⁺, 527.2224; found, 527.2167.

2-Chloro-6-propyl-4-(3-(trifluoromethyl)-5,6-dihydro-[1,2,4]triazolo[4,3-*a*]pyrazin-7(8*H*)-yl)thieno[2,3-*d*]pyrimidine (9). A solution of 2,4-dichloro-6-propylthieno[2,3-*d*]pyrimidine (1.05 g, 4.25 mmol), 3-(trifluoromethyl)-5,6,7,8-tetrahydro-[1,2,4]triazolo[4,3-*a*]pyrazine-HCl (1.09 g, 4.77 mmol), and DIPEA (2.5 mL, 14 mmol) in DMF (5 mL) was heated at 100 °C for 16 h. The solution was poured into ice-cold water, and the white precipitate was collected by filtration. The precipitate was washed with ice-cold water (2 × 20 mL) and dried in vacuo to yield compound **9** as a white solid (1.4 g, 3.5 mmol, 82%). ¹H NMR (500.27 MHz, CDCl₃): δ 7.04 (s, 1H), 5.36 (s, 2H), 4.39 (m, 4H), 2.88 (t, 2H, *J* = 7.0 Hz), 1.79 (h, 2H, *J* = 7.5 Hz), 1.01 (t, 3H, *J* = 7.3 Hz); ¹³C NMR (125.81 MHz, CDCl₃): δ 170.62, 157.59, 153.87, 149.93, 145.14, 119.34 (q, *J* = 270 Hz), 115.81, 115.25, 45.11, 43.00, 42.47, 33.17, 24.45, 13.74; ESI-HRMS: calcd for C₁₅H₁₅ClF₃N₆S [M + H]⁺, 403.0714; found, 403.0723.

2-(2-Fluoroethoxy)-6-propyl-4-(3-(trifluoromethyl)-5,6-dihydro-[1,2,4]triazolo[4,3-*a*]pyrazin-7(8*H*)-yl)thieno[2,3-*d*]pyrimidine (3). A suspension of compound **9** (0.11 g, 0.28 mmol), Cs₂CO₃ (0.14 g, 0.42 mmol), BINAP (22 mg, 35 μmol), palladium acetate (8.0 mg, 35 μmol), and 2-fluoroethanol (25 μL, 0.42 mmol) was heated to reflux for 4 h. After cooling to rt, the mixture was filtered over Celite, and the filtrate was concentrated in vacuo. Flash column chromatography (Hex/EtOAc 1:1) afforded compound **3** as a white solid (20 mg, 46 μmol, 17%). ¹H NMR (500.27 MHz, CDCl₃): δ 6.96 (s, 1H), 5.32 (s, 2H), 4.84 (m, 1H), 4.75 (m, 1H), 4.66 (m, 1H), 4.61 (m, 1H), 4.34 (m, 4H), 2.84 (t, 2H, *J* = 7.5 Hz), 1.76 (q, 2H, *J* = 7.5 Hz), 1.03 (t, 3H, *J* = 7.4 Hz); ¹³C NMR (125.81 MHz, CDCl₃): δ 171.35, 160.55, 158.61, 150.34, 141.43, 119.40, 115.26,

113.21, 81.74 (d, *J* = 169.9 Hz), 66.37, 45.14, 43.12, 42.60, 33.12, 24.49, 13.77; ESI-HRMS: calcd for C₁₇H₁₉F₄N₆OS [M + H]⁺, 431.1272; found, 431.1263.

Radiochemistry. Ethyl 6-(3-(3-((5-Chlorothiophen-2-yl)sulfonyl)[¹¹C]ureido)azetidin-1-yl)-5-cyano-2-methylnicotinate ([¹¹C]**1**). Compound [¹¹C]**1** was prepared as described previously.²⁰ Starting with approximately 25 GBq of [¹¹C]CO₂, the formulated product was obtained in a decay-corrected radiochemical yield of 17 ± 4% (966 ± 208 MBq) with a radiochemical purity of > 99%, a molar activity of 82 ± 28 GBq/μmol (*n* = 3) at the end of the synthesis, and an overall synthesis time of 45 min from the start of the synthesis. The identity of the product was confirmed with analytical HPLC by co-injection of the product and non-labeled **1**.

4-(4-(4-([1,1'-Biphenyl]-4-¹¹C]carbonyl)piperazin-1-yl)-6-ethylthieno[2,3-*d*]pyrimidin-2-yl)piperazin-2-one ([¹¹C]**2**). [¹¹C]CO₂ was produced by the ¹⁴N(p,α)¹¹C nuclear reaction performed in a 0.5% O₂/N₂ gas mixture using an IBA Cyclone 18/9 cyclotron (IBA, Louvain-la-Neuve, Belgium). Radioactivity levels were measured using a Veenstra (Joure, The Netherlands) VDC-405 dose calibrator. Radiosyntheses were performed in an in-house-built remotely controlled synthesis unit.²⁷ After target gas irradiation, [¹¹C]CO₂ was concentrated on a silica trap (−196 °C, 50 mg silica gel, 100/80 mesh). When the activity reached a maximum, the trap was heated, and [¹¹C]CO₂ was passed over a gas purifier column (400 × 4 mm, silica gel, 100/80 mesh) using helium (30 mL·min^{−1}) as a carrier gas. The purified [¹¹C]CO₂ was passed over a molybdenum (150 μm, 99.99%) reductor column heated at 850 °C after which unreacted [¹¹C]CO₂ was trapped on an Ascarite column, and [¹¹C]CO was collected on a silica trap (−196 °C, 1 mg of silica gel, 100/80 mesh). The transfer gas was switched from helium to xenon (Fluka, ≥99.995). [¹¹C]CO was released by heating the trap and transferring by a gentle xenon flow (2.0 mL/min) to the previously charged and sealed reagent vial [precursor **8** (6.6 mg, 10 μmol), Pd₂(dba)₃ (0.9 mg, 1.0 μmol), PPh₃ (2.6 mg, 10 μmol), and biphenyl iodide (10 μL, 0.14 mmol), in THF (0.70 mL)]. The reaction solution was heated at 130 °C for 5 min. The solution was subsequently cooled to 20 °C and quenched by the addition of water (0.70 mL). Purification was performed by preparative HPLC on an Alltima C18 column (5 μm, 250 mm × 10 mm) using a mixture of MeCN/H₂O/TFA (45/55/0.1, v/v/v) at a flow rate of 4 mL/min (*R*_t: 15 min). The product was obtained ready for injection by reformulation of the preparative HPLC product fraction using a tC18 plus solid-phase extraction cartridge (Waters, Milford, MA, USA). The cartridge, preconditioned with 5 mL of ethanol and 5 mL of water, was loaded with the diluted preparative HPLC product fraction (approximately 6 mL of product fraction diluted with 40 mL of H₂O). The cartridge was then washed with 10 mL of water, followed by elution of the product from the cartridge with ethanol (1 mL). The ethanol fraction was diluted to 10% ethanol by the addition of saline (9 mL). Yields were decay-corrected to start the synthesis and determined based on the starting amount of [¹¹C]CO₂. Compound [¹¹C]**2** was obtained in a radiochemical yield of 10 ± 3% in a total synthesis time of 40 min. After formulation, 578 ± 93 MBq of product was obtained with a radiochemical purity of > 99% and a molar activity of 93 ± 49 GBq/μmol (*n* = 3). The identity of the radiolabeled product was confirmed by analytical (HPLC Platinum C18, MeCN/H₂O/TFA 50:50:0.1, *R*_t: 11 min) analysis by co-injection of both labeled and unlabeled compounds.

2-(2-[¹⁸F]Fluoroethoxy)-6-propyl-4-(3-(trifluoromethyl)-5,6-dihydro-[1,2,4]triazolo[4,3-*a*]pyrazin-7(8*H*)-yl)thieno[2,3-*d*]pyrimidine ([¹⁸F]**3**). After target irradiation, the [¹⁸F]fluoride ion was trapped on a PS-HCO₃[−] anion-exchange column (ABX, Radenberg, Germany). Elution of fluoride from the exchange column into a 3 mL screw-cap reaction vessel was performed with 1 mL of acetonitrile/water (9/1, v/v) containing Kryptofix 2.2.2 (13.0 mg, 34.6 μmol, 4,7,13,16,21,24-hexaoxa-1,10-diazabicyclo[8.8.8]hexacosane) and potassium carbonate (2.0 mg, 15 μmol). The solution was evaporated to dryness under a helium flow (50 mL·min^{−1}) and reduced pressure at 100 °C. Then, acetonitrile (1.0 mL) was added, and the solution was again evaporated to dryness employing the same conditions as described

above. After drying, a solution of ethylene carbonate (40 mg, 0.45 mmol) in a mixture of diethylene glycol and 1,2-dichlorobenzene (0.30 mL, 1:4, v/v) was added, and the solution was heated at 165 °C for 15 min. Distillation of the formed 2-fluoroethanol was performed at the same temperature using a helium flow of 10 mL·min⁻¹ and trapped in a second reaction vial, charged with the precursor **9** (1.0 mg, 2.5 μmol) and sodium hydride (60% dispersion in mineral oil, 5.0 mg, 0.13 mmol) in THF (300 μL). After completion of the distillation (approximately 15 min), the mixture was heated to 60 °C and stirred for 20 min prior to cooling to room temperature (rt) and dilution with water (1 mL). Purification was performed on a Phenomenex Luna C18 column (10 μm, 250 mm × 10 mm) using MeCN/H₂O/TFA (50:50:0.1, v/v/v) as a mobile phase at a flow rate of 4 mL/min (R_t: 16.5 min). The product fraction was diluted with water (40 mL) and passed over a preconditioned tC18 plus solid-phase extraction cartridge (Waters, Milford, MA, USA). After washing the cartridge with water (10 mL), the product was eluted with ethanol (1 mL) and saline (9 mL) to obtain the product ready for injection. As such, [¹⁸F] **3** was obtained in a 9 ± 2% yield (decay-corrected to start the synthesis) in a total synthesis time of 90 min (958 ± 44 MBq). The molar activity was 70 ± 14 GBq/μmol at the end of the synthesis. The radiochemical purity was >99%, and no chemical contaminants were observed (*n* = 3). The identity of the product was confirmed by co-injection of the unlabeled reference standard on a Grace Platinum C18 column (5 μm, 250 mm × 4.6 mm using MeCN/H₂O/TFA (55:45:0.1, v/v/v, R_t: 8.5 min).

Log D_{7,4} Determination. The partitioning of the PET tracers between 1-octanol and 0.2 M phosphate buffer (pH = 7.4) was determined by vigorously mixing the respective formulated PET tracer (50–100 μL, 5–10 MBq) with a solution of 0.2 M phosphate buffer (2 mL, pH 7.4) and 1-octanol (2 mL) for 1 min using a vortex apparatus. After a settling period of 1 h, three samples of 100 μL were taken from both layers. The samples were counted for radioactivity, and the log D_{7,4} values were calculated according to the following formula: $\log D_{7,4} = \log(A_{\text{oct}}/A_{\text{phosphate buffer}})$, where A_{oct} and A_{phosphate buffer} represent the average radioactivities of three 1-octanol and three phosphate buffer samples, respectively. The results are expressed as mean ± standard deviation (*n* = 3).

PET Scanning. Dynamic PET imaging was performed using dedicated small animal NanoPET/CT and NanoPET/MR scanners (Mediso Ltd., Hungary, Budapest) with identical PET components. Wistar rats (male, 12–15 weeks old, 250–350 g) were anesthetized with 4 and 2% isoflurane in 1 L·min⁻¹ O₂ for induction and maintenance, respectively. Rats were positioned on the scanner bed, and the respiratory rate was monitored for the duration of the scan, adjusting anesthesia when required. A dynamic PET scan was acquired immediately after intravenous (iv) administration (tail vein) of the PET tracers (10–25 MBq). For efflux blocking experiments, rats received tariquidar slowly by iv administration 30 min prior to tracer injection (15 mg·kg⁻¹, formulated as 3.75 mg/mL tariquidar in 2.5% (g/v) aqueous dextrose solution). For the P2Y₁₂R blocking experiments, unlabeled **3** (5 mg/kg) was co-administered with tariquidar (15 mg/kg). Reconstruction was performed using a fully three-dimensional reconstruction algorithm (Tera-TomoTM, Mediso Ltd.) with four iterations and six subsets, and an isotropic 0.4 mm voxel dimension. Data was analyzed using Amide (<http://amide.sourceforge.net>) or VivoQuant by manually drawing a region of interest around the full brain. Results are expressed as standardized uptake values [percentage injected dose per gram (% ID/g) normalized to body weight]. Error bars indicate the standard deviations.

In Vitro Autoradiography. Autoradiography was performed on flash-frozen rat brain sections (10 μm thickness). The sections were washed with 50 mM Tris-HCl buffer (pH 7.4) for 15 min. After drying under a gentle air flow, the sections were incubated with [¹⁸F] **3** (0.1 MBq·mL⁻¹) in 50 mM Tris-HCl with 3% BSA, pH 7.4, in the absence or presence of a P2Y₁₂R inhibitor at 1 μM concentration for 30 min. Washing was performed with cold Tris-HCl (5 mM, 4 °C, twice for 1 min), followed by dipping in ice-cold water. After drying in an air stream, rat brain sections were exposed to a phosphor imaging

screen (GE Healthcare, Buckinghamshire, UK) for 10 min and developed on a Typhoon FLA 7000 phosphor imager (GE Healthcare, Buckinghamshire, UK). Visualization of binding was performed using ImageQuantTL v8.1.0.0 (GE Healthcare, Buckinghamshire, UK). Quantification was performed by a region of interest of the whole brain area. Results are expressed as % of binding relative to the baseline condition where no P2Y₁₂R inhibitor was used. Error bars indicate the standard deviation.

Biodistribution and Metabolite Analysis. Rats were sacrificed after PET scanning (60 min after tracer injection), and organs and tissues were collected, weighed, and counted in a gamma counter. In addition, blood was collected by arterial puncture (approximately 1 mL) and transferred to a heparin-coated Eppendorf tube. Blood samples were centrifuged for 5 min at 4600 rpm to separate blood plasma from cells. The plasma (100 μL) was diluted in acetonitrile (200 μL at 0 °C) and centrifuged for 5 min at 15,000 rpm for removal of proteins. Brain hemispheres were homogenized in acetonitrile (200 μL at 0 °C) and centrifuged for 5 min at 15,000 rpm. An aliquot of each supernatant (10 μL) was transferred to a TLC plate, which was subsequently dried at rt for 5 min and ran in a solution of DCM/MeOH (9:1, v/v). The radioTLC plate was transferred to a phosphor imager storage screen and left for 1 h. Readout was performed on a Typhoon phosphor imager, and subsequent analysis was performed using ImageQuant. Results are expressed as average ± standard deviation (*n* = 4).

Statistical Analysis. Where appropriate, statistical analysis was performed using Student's *t*-test using GraphPad Prism Version 9.1.0.

■ ASSOCIATED CONTENT

Supporting Information

The Supporting Information is available free of charge at <https://pubs.acs.org/doi/10.1021/acschemneuro.1c00641>.

Preparative and analytical HPLC chromatograms of [¹⁸F] **3**; radioTLC analysis of blood and brain extracts after [¹⁸F] **3** administration; CNS-MPO and CNS-PET-MPO scores for developed PET tracers; ex vivo biodistribution results after [¹⁸F] **3** administration; and ¹H NMR, ¹³C NMR, and ESI-HRMS spectra of compounds (PDF)

■ AUTHOR INFORMATION

Corresponding Author

Berend van der Wildt – Department of Radiology & Nuclear Medicine, Neuroscience Amsterdam, Amsterdam UMC, Vrije Universiteit Amsterdam, 1081HV Amsterdam, The Netherlands; orcid.org/0000-0001-5503-2382; Email: b.vanderwildt@amsterdamumc.nl

Authors

Bieneke Janssen – Department of Radiology & Nuclear Medicine, Neuroscience Amsterdam, Amsterdam UMC, Vrije Universiteit Amsterdam, 1081HV Amsterdam, The Netherlands; orcid.org/0000-0001-9573-8558

Aleksandra Pekošak – Department of Radiology & Nuclear Medicine, Neuroscience Amsterdam, Amsterdam UMC, Vrije Universiteit Amsterdam, 1081HV Amsterdam, The Netherlands

E. Johanna L. Stéen – Department of Radiology & Nuclear Medicine, Neuroscience Amsterdam, Amsterdam UMC, Vrije Universiteit Amsterdam, 1081HV Amsterdam, The Netherlands

Robert C. Schuit – Department of Radiology & Nuclear Medicine, Neuroscience Amsterdam, Amsterdam UMC, Vrije Universiteit Amsterdam, 1081HV Amsterdam, The Netherlands

Esther J. M. Kooijman – Department of Radiology & Nuclear Medicine, Neuroscience Amsterdam, Amsterdam UMC, Vrije Universiteit Amsterdam, 1081HV Amsterdam, The Netherlands

Wissam Beaino – Department of Radiology & Nuclear Medicine, Neuroscience Amsterdam, Amsterdam UMC, Vrije Universiteit Amsterdam, 1081HV Amsterdam, The Netherlands

Danielle J. Vugts – Department of Radiology & Nuclear Medicine, Neuroscience Amsterdam, Amsterdam UMC, Vrije Universiteit Amsterdam, 1081HV Amsterdam, The Netherlands; orcid.org/0000-0001-7068-8152

Albert D. Windhorst – Department of Radiology & Nuclear Medicine, Neuroscience Amsterdam, Amsterdam UMC, Vrije Universiteit Amsterdam, 1081HV Amsterdam, The Netherlands; orcid.org/0000-0002-1250-7656

Complete contact information is available at:

<https://pubs.acs.org/10.1021/acscchemneuro.1c00641>

Author Contributions

B.v.d.W. and B.J. contributed equally. B.v.d.W., B.J., A.P., and E.J.L.S. have performed the chemical and radiochemical synthesis. B.v.d.W., B.J., W.B., and E.J.M.K. designed and performed the animal experiments. B.v.d.W. and R.C.S. have performed the radiometabolite analysis. D.J.V. and A.D.W. have supervised the project. B.v.d.W. wrote the manuscript. All authors have carefully read the final version of the manuscript and agreed with its contents.

Notes

The authors declare the following competing financial interest(s): A.D. Windhorst is editor-in-chief of Nuclear Medicine and Biology, other authors have no conflict of interest.

ACKNOWLEDGMENTS

The research leading to these results has received funding from the Michael J. Fox Foundation (Triple-P, grant number 12274, B.J. and A.P.), the European Union's Horizon 2020 research and innovation program as a Marie Skłodowska–Curie Individual Fellowship under grant agreement no. 892572 (E.J.L.S.), and NWO (Dutch Research Council) as a NWO-VENI grant under grant number VI.Veni.192.229 (B.v.d.W.).

REFERENCES

- (1) Michell-Robinson, M. A.; Touil, H.; Healy, L. M.; Owen, D. R.; Durafour, B. A.; Bar-Or, A.; Antel, J. P.; Moore, C. S. Roles of microglia in brain development, tissue maintenance and repair. *Brain* **2015**, *138*, 1138–1159.
- (2) Li, Q.; Barres, B. A. Microglia and macrophages in brain homeostasis and disease. *Nat. Rev. Immunol.* **2018**, *18*, 225–242.
- (3) Kettenmann, H.; Hanisch, U.-K.; Noda, M.; Verkhratsky, A. Physiology of microglia. *Physiol. Rev.* **2011**, *91*, 461–553.
- (4) Colonna, M.; Butovsky, O. Microglia function in the central nervous system during health and neurodegeneration. *Annu. Rev. Immunol.* **2017**, *35*, 441–468.
- (5) Salter, M. W.; Stevens, B. Microglia emerge as central players in brain disease. *Nat. Med.* **2017**, *23*, 1018–1027.
- (6) DiSabato, D. J.; Quan, N.; Godbout, J. P. Neuroinflammation: the devil is in the details. *J. Neurochem.* **2016**, *139*, 136–153.
- (7) Fumagalli, M.; Lombardi, M.; Gressens, P.; Verderio, C. How to reprogram microglia toward beneficial functions. *Glia* **2018**, *66*, 2531–2549.
- (8) Yang, S.; Qin, C.; Hu, Z.-W.; Zhou, L.-Q.; Yu, H.-H.; Chen, M.; Bosco, D. B.; Wang, W.; Wu, L.-J.; Tian, D.-S. Microglia reprogram

metabolic profiles for phenotype and function changes in central nervous system. *Neurobiol. Dis.* **2021**, *152*, 105290.

(9) Werry, E. L.; Bright, F. M.; Piguet, O.; Ittner, L. M.; Halliday, G. M.; Hodges, J. R.; Kiernan, M. C.; Loy, C. T.; Kril, J. J.; Kassiou, M. Recent developments in TSPO PET imaging as a biomarker of neuroinflammation in neurodegenerative disorders. *Int. J. Mol. Sci.* **2019**, *20*, 3161.

(10) Janssen, B.; Vugts, D.; Windhorst, A.; Mach, R. PET Imaging of Microglial Activation-Beyond Targeting TSPO. *Molecules* **2018**, *23*, 607.

(11) Beaino, W.; Janssen, B.; Vugts, D. J.; de Vries, H. E.; Windhorst, A. D. Towards PET imaging of the dynamic phenotypes of microglia. *Clin. Exp. Immunol.* **2021**, *206*, 282.

(12) Janssen, B.; Vugts, D. J.; Funke, U.; Spaans, A.; Schuit, R. C.; Kooijman, E.; Rongen, M.; Perk, L. R.; Lammertsma, A. A.; Windhorst, A. D. Synthesis and initial preclinical evaluation of the P2X₇ receptor antagonist [¹¹C]A740003 as a novel tracer of neuroinflammation. *J. Labelled Compd. Radiopharm.* **2014**, *57*, S09–S16.

(13) Gao, M.; Wang, M.; Green, M. A.; Hutchins, G. D.; Zheng, Q.-H. Synthesis of [¹¹C]GSK1482160 as a new PET agent for targeting P2X₇ receptor. *Bioorg. Med. Chem. Lett.* **2015**, *25*, 1965–1970.

(14) Ory, D.; Celen, S.; Gijsbers, R.; van Den Haute, C.; Postnov, A.; Koole, M.; Vandeputte, C.; Andrés, J.-L.; Alcazar, J.; De Angelis, M.; Langlois, X.; Bhattacharya, A.; Schmidt, M.; Letavic, M. A.; Vanduffel, W.; van Laere, K.; Verbruggen, A.; Debyser, Z.; Bormans, G. Preclinical evaluation of a P2X₇ receptor-selective radiotracer: PET studies in a rat model with local overexpression of the human P2X₇ receptor and in nonhuman primates. *J. Nucl. Med.* **2016**, *57*, 1436–1441.

(15) Territo, P. R.; Meyer, J. A.; Peters, J. S.; Riley, A. A.; McCarthy, B. P.; Gao, M.; Wang, M.; Green, M. A.; Zheng, Q.-H.; Hutchins, G. D. Characterization of ¹¹C-GSK1482160 for targeting the P2X₇ receptor as a biomarker for neuroinflammation. *J. Nucl. Med.* **2017**, *58*, 458–465.

(16) Han, J.; Liu, H.; Liu, C.; Jin, H.; Perlmutter, J. S.; Egan, T. M.; Tu, Z. Pharmacologic characterizations of a P2X₇ receptor-specific radioligand, [¹¹C]GSK1482160 for neuroinflammatory response. *Nucl. Med. Commun.* **2017**, *38*, 372–382.

(17) Janssen, B.; Vugts, D. J.; Wilkinson, S. M.; Ory, D.; Chalon, S.; Hoozemans, J. J. M.; Schuit, R. C.; Beaino, W.; Kooijman, E. J. M.; van den Hoek, J.; Chishty, M.; Doméné, A.; van der Perren, A.; Villa, A.; Maggi, A.; Molenaar, G. T.; Funke, U.; Shevchenko, R. V.; Baekelandt, V.; Bormans, G.; Lammertsma, A. A.; Kassiou, M.; Windhorst, A. D. Identification of the allosteric P2X₇ receptor antagonist [¹¹C]SMW139 as a PET tracer of microglial activation. *Sci. Rep.* **2018**, *8*, 6580.

(18) Beaino, W.; Janssen, B.; Kooijman, E.; Vos, R.; Schuit, R. C.; O'Brien-Brown, J.; Kassiou, M.; van het Hof, B.; Vugts, D. J.; de Vries, H. E.; Windhorst, A. D. PET imaging of P2X₇R in the experimental autoimmune encephalomyelitis model of multiple sclerosis using [¹¹C]SMW139. *J. Neuroinflammation* **2020**, *17*, 300.

(19) Hagens, M. H. J.; Golla, S. S. V.; Janssen, B.; Vugts, D. J.; Beaino, W.; Windhorst, A. D.; O'Brien-Brown, J.; Kassiou, M.; Schuit, R. C.; Schwarte, L. A.; de Vries, H. E.; Killestein, J.; Barkhof, F.; van Berckel, B. N. M.; Lammertsma, A. A. The P2X₇ receptor tracer [¹¹C]SMW139 as an in vivo marker of neuroinflammation in multiple sclerosis: a first-in man study. *Eur. J. Nucl. Med. Mol. Imag.* **2020**, *47*, 379–389.

(20) Villa, A.; Klein, B.; Janssen, B.; Pedragosa, J.; Pepe, G.; Zinnhardt, B.; Vugts, D. J.; Gelosa, P.; Sironi, L.; Beaino, W.; Damont, A.; Dollé, F.; Jego, B.; Winkler, A.; Ory, D.; Solin, O.; Vercouillie, J.; Funke, U.; Laner-Plamberger, S.; Blomster, L. V.; Christophersen, P.; Vegeto, E.; Aigner, L.; Jacobs, A.; Planas, A. M.; Maggi, A.; Windhorst, A. D. Identification of new molecular targets for PET imaging of the microglial anti-inflammatory activation state. *Theranostics* **2018**, *8*, 5400–5418.

(21) Mildner, A.; Huang, H.; Radke, J.; Stenzel, W.; Priller, J. P2Y₁₂ receptor is expressed on human microglia under physiological

conditions throughout development and is sensitive to neuro-inflammatory diseases. *Glia* **2017**, *65*, 375–387.

(22) Zhang, J.; Zhang, K.; Gao, Z.-G.; Paoletta, S.; Zhang, D.; Han, G. W.; Li, T.; Ma, L.; Zhang, W.; Müller, C. E.; Yang, H.; Jiang, H.; Cherezov, V.; Katritch, V.; Jacobson, K. A.; Stevens, R. C.; Wu, B.; Zhao, Q. Agonist-bound structure of the human P2Y₁₂ receptor. *Nature* **2014**, *509*, 119–122.

(23) Zhang, K.; Zhang, J.; Gao, Z.-G.; Zhang, D.; Zhu, L.; Han, G. W.; Moss, S. M.; Paoletta, S.; Kiselev, E.; Lu, W.; Fenalti, G.; Zhang, W.; Müller, C. E.; Yang, H.; Jiang, H.; Cherezov, V.; Katritch, V.; Jacobson, K. A.; Stevens, R. C.; Wu, B.; Zhao, Q. Structure of the human P2Y₁₂ receptor in complex with an antithrombotic drug. *Nature* **2014**, *509*, 115–118.

(24) Moore, C. S.; Ase, A. R.; Kinsara, A.; Rao, V. T. S.; Michell-Robinson, M.; Leong, S. Y.; Butovsky, O.; Ludwin, S. K.; Séguéla, P.; Bar-Or, A.; Antel, J. P. P2Y₁₂ expression and function in alternatively activated human microglia. *Neurol. Neuroimmunol. Neuroinflammation* **2015**, *2*, No. e80.

(25) Pharmacia & Upjohn company LLC. 4-piperazinylthieno [2,3-d] pyrimidine compounds as platelet aggregation inhibitors. WO 2006103544 A2, 2006.

(26) LG Life Sciences LTD. Fused heterocyclic compound. WO 2010027236, 2010.

(27) Eriksson, J.; van den Hoek, J.; Windhorst, A. D. Transition metal mediated synthesis using [¹¹C]CO at low pressure – a simplified method for ¹¹C-carboxylation. *J. Labelled Compd. Radiopharm.* **2012**, *55*, 223–228.

(28) Pan, J.; Pourghasian, M.; Hundal, N.; Lau, J.; Bénard, F.; Dedhar, S.; Lin, K.-S. 2-[¹⁸F]Fluoroethanol and 3-[¹⁸F]-fluoropropanol: facile preparation, biodistribution in mice, and their application as nucleophiles in the synthesis of [¹⁸F]fluoroalkyl aryl ester and ether PET tracers. *Nucl. Med. Biol.* **2013**, *40*, 850–857.

(29) Bankstahl, J. P.; Kuntner, C.; Abraham, A.; Karch, R.; Stanek, J.; Wanek, T.; Wadsak, W.; Kletter, K.; Müller, M.; Löscher, W.; Langer, O. Tariquidar-induced P-glycoprotein inhibition at the rat bloodbrain barrier studied with (R)-¹¹C-verapamil and PET. *J. Nucl. Med.* **2008**, *49*, 1328–1335.

(30) Bankstahl, J. P.; Bankstahl, M.; Römermann, K.; Wanek, T.; Stanek, J.; Windhorst, A. D.; Fedrowitz, M.; Erker, T.; Müller, M.; Löscher, W.; Langer, O.; Kuntner, C. Tariquidar and elacridar are dose-dependently transported by P-glycoprotein and Bcrp at the blood-brain barrier: a small-animal positron emission tomography and in vitro study. *Drug Metab. Dispos.* **2013**, *41*, 754–762.

(31) Bach, P.; Boström, J.; Brickmann, K.; van Giezen, J. J. J.; Groneberg, R. D.; Harvey, D. M.; O'Sullivan, M.; Zetterberg, F. Synthesis, structure-property relationships and pharmacokinetic evaluation of ethyl 6-aminonicotinate sulfonylureas as antagonists of the P2Y₁₂ receptor. *Eur. J. Med. Chem.* **2013**, *65*, 360–375.

(32) Bach, P.; Boström, J.; Brickmann, K.; van Giezen, J. J. J.; Hovland, R.; Petersson, A. U.; Ray, A.; Zetterberg, F. A novel series of piperazinyl-pyridine ureas as antagonists of the purinergic P2Y₁₂ receptor. *Bioorg. Med. Chem. Lett.* **2011**, *21*, 2877–2881.

(33) Wager, T. T.; Hou, X.; Verhoest, P. R.; Villalobos, A. Moving beyond rules: the development of a central nervous system multiparameter optimization (CNS MPO) approach to enable alignment of druglike properties. *ACS Chem. Neurosci.* **2010**, *1*, 435–449.

(34) Zhang, L.; Villalobos, A.; Beck, E. M.; Bocan, T.; Chappie, T. A.; Chen, L.; Grimwood, S.; Heck, S. D.; Helal, C. J.; Hou, X.; Humphrey, J. M.; Lu, J.; Skaddan, M. B.; McCarthy, T. J.; Verhoest, P. R.; Wager, T. T.; Zasadny, K. Design and selection parameters to accelerate the discovery of novel central nervous system positron emission tomography (PET) ligands and their application in the development of a novel phosphodiesterase 2A PET ligand. *J. Med. Chem.* **2013**, *56*, 4568–4579.

(35) Syvänen, S.; Lindhe, Ö.; Palner, M.; Kornum, B. R.; Rahman, O.; Långström, B.; Knudsen, G. M.; Hammarlund-Udenaes, M. Species differences in blood-brain barrier transport of three positron

emission tomography radioligands with emphasis on P-glycoprotein transport. *Drug Metab. Dispos.* **2009**, *37*, 635–643.

(36) Shalgunov, V.; Xiong, M.; L'Estrade, E. T.; Raval, N. R.; Andersen, I. V.; Edgar, F. G.; Speth, N. R.; Baerentzen, S. L.; Hansen, H. D.; Donovan, L. L.; Nasser, A.; Peitersen, S. T.; Kjaer, A.; Knudsen, G. M.; Syvänen, S.; Palner, M.; Herth, M. M. Blocking of efflux transporters in rats improves translational validation of brain radioligands. *EJNMMI Res.* **2020**, *10*, 124.

(37) Koski, R.; Kennedy, B. Comparative review of oral P2Y₁₂ inhibitors. *Pharm. Therapeut.* **2018**, *43*, 352–357.

(38) Beaino, W.; Janssen, B.; Kooij, G.; van der Pol, S. M. A.; van Het Hof, B.; van Horsen, J.; Windhorst, A. D.; de Vries, H. E. Purinergic receptors P2Y₁₂R and P2X₇R: potential targets for PET imaging of microglia phenotypes in multiple sclerosis. *J. Neuroinflammation* **2017**, *14*, 259.

(39) Coenen, H. H.; Gee, A. D.; Adam, M.; Antoni, G.; Cutler, C. S.; Fujibayashi, Y.; Jeong, J. M.; Mach, R. H.; Mindt, T. L.; Pike, V. W.; Windhorst, A. D. Consensus nomenclature rules for radiopharmaceutical chemistry — Setting the record straight. *Nucl. Med. Biol.* **2017**, *55*, v–xi.